Cancer Research

Inhibition of Pyruvate Dehydrogenase Kinase Enhances the Antitumor Efficacy of Oncolytic Reovirus

Barry E. Kennedy[1], John Patrick Murphy[1], Derek R. Clements[1], Prathyusha Konda[2], Namit Holay[1], Youra Kim[1], Gopal P. Pathak[1], Michael A. Giacomantonio[1], Yassine El Hiani[3], and Shashi Gujar[1,2,4,5]

Abstract

Oncolytic viruses (OV) such as reovirus preferentially infect and kill cancer cells. Thus, the mechanisms that dictate the susceptibility of cancer cells to OV-induced cytotoxicity hold the key to their success in clinics. Here, we investigated whether cancer cell metabolism defines its susceptibility to OV and if OV-induced metabolic perturbations can be therapeutically targeted. Using mass spectrometry–based metabolomics and extracellular flux analysis on a panel of cancer cell lines with varying degrees of susceptibility to reovirus, we found that OV-induced changes in central energy metabolism, pyruvate metabolism, and oxidative stress correlate with their susceptibility to reovirus. In particular, reovirus infection accentuated Warburg-like metabolic perturbations in cell lines relatively resistant to oncolysis. These metabolic changes were facilitated by oxidative stress–induced inhibitory phosphorylation of pyruvate dehydrogenase (PDH) that impaired the routing of pyruvate into the tricarboxylic acid cycle and established a metabolic state unsupportive of OV replication. From the therapeutic perspective, reactivation of PDH in cancer cells that were weakly sensitive for reovirus, either through PDH kinase (PDK) inhibitors dichloroacetate and AZD7545 or short hairpin RNA–specific depletion of PDK1, enhanced the efficacy of reovirus-induced oncolysis *in vitro* and *in vivo*. These findings identify targeted metabolic reprogramming as a possible combination strategy to enhance the antitumor effects of OV in clinics.

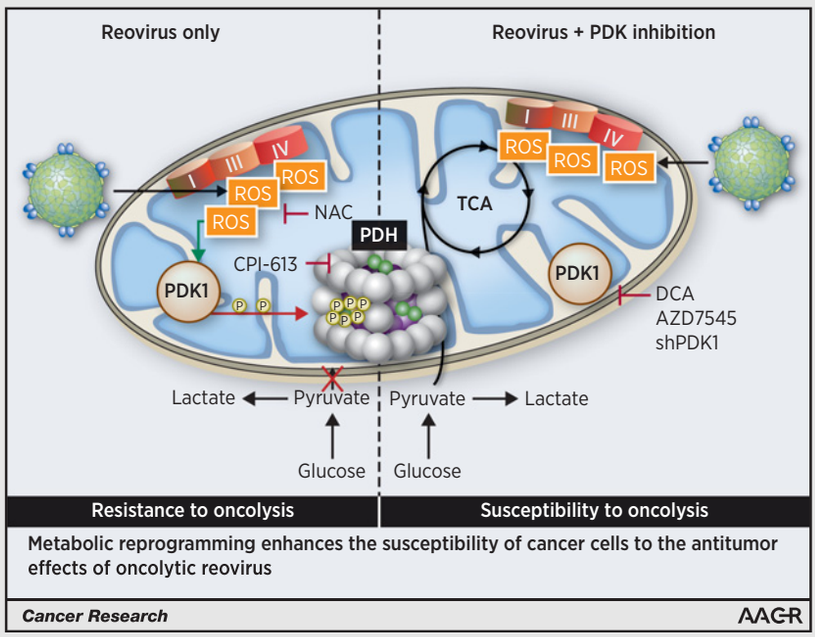

Significance: This study proposes targeted metabolic reprogramming as a valid combinatorial strategy to enhance the translational efficacy of oncolytic virus–based cancer therapies.

Graphical Abstract: http://cancerres.aacrjournals.org/content/canres/79/15/3824/F1.large.jpg.

[1]Department of Pathology, Dalhousie University, Halifax, Nova Scotia, Canada. [2]Department Microbiology and Immunology, Dalhousie University, Halifax, Nova Scotia, Canada. [3]Department Physiology and Biophysics, Dalhousie University, Halifax, Nova Scotia, Canada. [4]Department Biology, Dalhousie University, Halifax, Nova Scotia, Canada. [5]Centre for Innovative and Collaborative Health Systems Research, IWK Health Centre, Halifax, Nova Scotia, Canada.

Note: Supplementary data for this article are available at Cancer Research Online (http://cancerres.aacrjournals.org/).

Corresponding Author: Shashi Gujar, Dalhousie University, Faculty of Medicine, Sir Charles Tupper Building, Halifax, Nova Scotia B3H 1X5, Canada. Phone: 902-494-2787; Fax: 902-494-3292; E-mail: shashi.gujar@dal.ca

Cancer Res 2019;79:3824–36

doi: 10.1158/0008-5472.CAN-18-2414

Introduction

Oncolytic viruses (OV) preferentially infect and kill cancer cells, in a process known as oncolysis, without harming normal cells. As such, many OVs are being tested internationally in phase I/II/III clinical trials (1). One such oncolytic agent, reovirus, a benign double-stranded human RNA virus, is known to preferentially infect and lyse a wide range of cancerous cells in preclinical models, and in patients (2, 3). Cancer cells with impaired expression of IFN show heightened permissiveness to reovirus infection (4). Once inside, the mechanism of reovirus-induced cytotoxicity is less clear, but necrosis, apoptosis, and autophagy are all likely involved (5, 6). It is being acknowledged that the optimum therapeutic efficacy of OV will depend on the complimentary therapeutic interventions that synergize its antitumor effects.

For over 50 years, it has been known that, following virus infection, the generation of viral particles in the infected cell is facilitated through intrinsic metabolic pathways (7). Paradoxically, cellular antiviral defenses employ similar metabolic changes, such as upregulation of glycolysis, to fight viral infection through an unclear mechanism (8, 9). In this context, a better understanding of the metabolic perturbations arising due to OV infection of cancer cells promise to unravel new therapeutically relevant vulnerabilities within cancers.

Here, using mass spectrometry–based metabolomics and extracellular flux analysis in several cancer cells, we show that susceptibility of cancer cells to reovirus-mediated oncolysis correlates with the perturbations within central energy metabolism and oxidative stress. In cancer cells that are relatively resistant to reovirus-mediated oncolysis, such as the triple-negative murine breast cancer cells, 4T1, reovirus infection causes an early induction of oxidative stress, which causes phosphorylation-dependent inhibition of pyruvate dehydrogenase (PDH), leading to a metabolic state unsupportive of OV replication and subsequent oncolysis. Most importantly, therapeutically relevant reactivation of PDH, through the pharmacologic or genetic inhibition of PDH kinase 1 (PDK1), enhances antitumor efficacy of reovirus *in vitro* and *in vivo*. In summary, these findings put forward a therapeutic paradigm, wherein, targeted metabolic manipulations can be combined with OVs to formulate the efficacious combinatorial cancer virotherapies.

Materials and Methods

Chemical and reagents

All chemicals and reagents were acquired from Sigma or Thermo Fisher Scientific, unless otherwise stated.

Animals

For the reovirus-only injections, 6- to 8-week-old female Balb/c mice were purchased from Charles River. 4T1 tumors were generated by injecting 1×10^5 cells per mouse in the right flank. Visible tumors (day 10 post injection) were injected with a series of three intratumoral injections of reovirus [5×10^8 plaque-forming unit (PFU), in 50 μL of PBS] each 2 days apart. Five mice per group were used. For the combination studies, 6- to 8-week-old female Balb/c mice were purchased from Charles River and male NOD SCID (NOD.CB17-Prkdcscid/NCrCrl) mice were generated by an in-house breeding colony. Ten- to 16-week-old SCID mice (2–5/cage) and Balb/c (4 or 5/cage) were injected with 5×10^4 4T1 cells in the right flank. Visible tumors (day 14 post injection for SCID and day 10 for Balb/c) were injected with a series of three intratumoral injections each 2 days apart, these injections were either PBS, DCA (50 mg/kg mouse), reovirus (5×10^8 PFU for Balb/c or 1×10^7 PFU for SCID), or combination of reovirus and DCA in a total volume of 50 μL. The mice were randomly treated but identical treatment groups were housed together for the duration of the experiment. In addition, 1 day after tumor injection, DCA was supplied in the drinking water at 500 mg/L (based on observation that SCID and Balb/c mice consumed an average of 5 and 2 mL of water per day per mouse, respectively; ref. 10), therefore each SCID mouse consumed approximately 100 mg/kg and each Balb/c mouse consumed approximately 40 mg/kg of DCA a day), this protocol was adopted from Yaromina and colleagues (11). In addition, chow mash was provided to all mice, and where applicable, mash was supplemented with DCA at 500 mg/L. Between 8 and 15 mice were used per group.

The ellipsoid volume formulas (pi/6 × longest diameter × smallest diameter × height of tumor) was measured every second day throughout the duration of the experiment with a caliper. The mice were monitored every day, and endpoints were determined unbiasedly by independent animal technicians according to tumor size, tumor ulceration, mouse weight loss, and mouse overall health. The experimental procedures were governed by the approval of the Ethics Committee at the Dalhousie University (Halifax, Nova Scotia, Canada).

Cell lines and reovirus

Reovirus (serotype 3, Dearing strain) was propagated in L929 cells grown in suspension in Joklik-modified Eagle medium containing 5% FBS. The virus was purified according to the protocol of Smith and colleagues (12) with the exception that β-mercaptoethanol was omitted from the extraction buffer. Dead virus was prepared by exposing the live virus to ultraviolet (UV) light for 45 minutes. Reovirus concentration was determined through titering virus on L929 cells by standard plaque assay.

Murine breast cancer (4T1), melanoma (B16-F10), teratocarcinoma (P19), pancreatic (Pan02), prostate (TRAMPC2), prostate (TRAMPC1), and human pancreatic (Panc1) cancer cells were originally purchased from ATCC. Mouse ovarian surface epithelial (ID8) cells were obtained from Edith Lord (University of Rochester, Rochester, NY; ref. 13). Further cell authentication was not performed for this study. Cells were grown and maintained as per ATCC protocols. *Mycoplasma* testing was performed bimonthly using MycoAlert (Lonza). Furthermore, all experiments were performed within 10 passages after thawing frozen stocks.

Mass spectrometry metabolomics

Samples were prepared and analyzed as per Yuan and colleagues (14). Cancer cells (grown to confluency in a 6-well plate) infected with or without reovirus [multiplicity of infection (MOI) 10] and treated with or without DCA (5 or 20 mmol/L) were collected in 200 μL of 80% ice -cold (−20°C) methanol. Metabolite levels were analyzed using multiple reaction monitoring with a Sciex 5500 QTRAP triple-quadrupole mass spectrometer. MultiQuant v2.1 software was used to integrate the peak areas from the Q3 TIC values across the chromatographic elution. Each peak area from every sample was manually confirmed. Peak heights normalized to the sum of peak heights per sample were used to determine relative metabolite concentrations between samples. Each relative metabolite level represents the mean of three samples from independent wells.

Proteomics

Trypsin-digested peptides were labeled using TMT 11-plex reagents as described previously (15). TMT11-labeled samples were fractionated using high-pH reverse-phase chromatography performed with an Onyx monolithic 100 × 4.6-mm C18 column (Phenomenex). Fractions were desalted using homemade Stage Tips (16), lyophilized, and analyzed with an Orbitrap Velos Mass Spectrometer (Thermo Fisher Scientific) using an MS3 method as described previously (15–17). Protein identification was performed using a database search against a mouse proteome database (downloaded from UniProtKB in September 2014) concatenated to a mammalian orthoreovirus 3 (Dearing strain) database (downloaded from UniProtKB in September 2014). All FDR filtering and protein quantitation was performed as described previously (15). A protein was required to have a minimum total signal-to-noise ratio of 100 in all TMT reporter channels. Data for heatmaps and individual protein profiles are represented by relative intensity, based on the summed signal-to-noise ratio.

Flow cytometry

Briefly, trypsinized cancer cells were incubated with a viability dye [7AAD (eBioscience catalog no. 00-6993-50, 1:50)] for 15 minutes at 4°C, reactive oxygen species stains [H2DCFH-DA (DCF, Molecular Probes catalog no. C6827, 1 μmol/L) or MitoSOX (Molecular Probes catalog no. M36008, 5 μmol/L)] for 30 minutes at 37°C for 30 minutes at 37°C in FACS buffer [PBS pH 7.4 (Gibco catalog no. 10010), 1% FBS, and 5 mmol/L EDTA] according to the manufacturer's protocol. To measure glucose uptake, cells were incubated with a fluorescent D-glucose analogue, 2-[N-(7-nitrobenz-2-oxa-1,3-diazol-4-yl) amino]-2-deoxy-D-glucose [2-NBDG #N13195 (50 μmol/L)], for 30 minutes at 37°C in normal media. For reovirus infectivity detection, trypsinized cancer cells were permeabilized and fixed using FOXP3 Fix/Perm Buffer (BioLegend catalog no. 421403). Permeabilized fixed cells were incubated with a rat anti-reovirus antibody (generated in-house) for 30 minutes at 4°C and subsequent secondary Alexa 488–conjugated anti-rat antibody (Invitrogen) for 30 minutes at 4°C. Data acquisition was done with BD FACSCalibur, data analysis was done using Flowing 2 or FCS Express V5 Software (De Novo Software). Each metabolic FACS experiment was completed a minimum of five independent experiments each completed in triplicate.

Metabolomic assays

Lactate assay was completed using a kit from Megazyme as per the manufacturer's protocol.

Extracellular flux analysis was completed with a XF24 Analyzer (Seahorse Biosciences). Briefly, 8×10^4 cancer cells were seeded into the XF24 cell culture microplate and incubated with or without DCA (5 or 20 mmol/L) and/or reovirus (MOI 1 or 10) for 24 hours. Oxygen consumption rate (OCR) and extracellular acidification rate (ECAR) by cells were measured in XF assay media (unbuffered DMEM containing 2 mmol/L glutamine and 1 mmol/L pyruvate) after subsequent injections of glucose (final = 10 mmol/L), oligomycin [O4876; Sigma (final) = 1 μmol/L], carbonyl cyanide 4-(trifluoromethoxy)phenylhydrazone [FCCP, C2920; Sigma (final) = 1.5 μmol/L], rotenone [R8875; Sigma (final) = 1 μmol/L], and antimycin A [A8674; Sigma (final) = 1 μmol/L] according to the manufacturer's protocol. After each experiment, live cells were counted by trypan blue exclusion and ECAR and OCR values were normalized, although minimal cell death was observed. For the initial cancer cell screen, all measurements were completed on three independent experiments. For 4T1 experiments, the Seahorse experiments were completed in five independent experiments all in triplicate.

Immunoblot analysis

Cell lysates were prepared in 0.1% SDS in PBS with protease and phosphatase inhibitors. Protein content was determined by a bicinchoninic acid–based Photometric Assay (Thermo Fisher Scientific catalog no. 23235). Proteins were separated by SDS-PAGE and transferred to nitrocellulose membranes. Membranes were blocked in 2% (w/v) BSA in TBS with 5% (v/v) Tween (pH 7.4). Primary antibodies used in this study were: mouse anti-pyruvate dehydrogenase e1-alpha subunit antibody (Abcam catalog no. ab110330), rabbit anti-pyruvate dehydrogenase e1-alpha subunit (phospho s293) antibody (Abcam catalog no. ab177461), rabbit anti-pdk1 (Cell Signaling Technology catalog no. c47h1), and mouse anti-beta-actin (Santa Cruz Biotechnology catalog no. sc-47778). Secondary horseradish peroxidase–conjugated donkey anti-rabbit and anti-mouse antibodies were detected by enhanced chemiluminescence. Imaging and analysis of band density was performed by Bio-Rad blot analyzer. For the pPDH analysis in all cancer cells we were unable to load all of the samples on a single gel, so to compare levels across immune blots we used an exposure control, all bands were normalized to the exposure control before ratios were calculated. Immunoblot analysis represents data from a minimum of three independent experiments.

qRT-PCR

RNA extractions were conducted using TRizol methodology. A Bio-Rad PCR machine was used for qRT-PCR, using GoTaq qPCR Master Mix (Promega) for amplification and quantification. All primers used were purchased from Invitrogen. Primers used (5′–3′): *Pdk1* (ACGGGACAGATGCGGTTATC and GCTTCCAGGCGGCTTTATTG), *Pdk2* (CGGGCGCTGTTGAAGAATG and CCTGCCGGAGGAAAGTGAAT), *Pdk3* (AAGCAGATCGAGCGCTACTC and TTAGCCAGTCGCACAGGAAG), *Pdk4* (TTTCCAGGCCAACCAATCCA and AGACGACAGTGGCCTCTACT), *Ddx58* AGACGGTTCACCGCATACAG and AAGCGTCTCCAAGGACAGTG), *Ifna1* (TTTCCCCTGACCCAGGAAGATG and TCTCTCAGTCTTCCCAGCACATT), and *Isg56* (GAGCCAGAAAACCCTGAGTACA and AGAAATAAAGTTGTCATCTAAATC). The results were collected and analyzed by Livak and Schmittgen $2-\Delta\Delta C_t$ method (18). All qPCR data were collected from three independent experiments.

Lentiviral short hairpin RNA knockdown

Lentiviral short hairpin RNA (shRNA) clones for *Pdk1* were from the RNAi consortium (Dharmacon catalog no. RMM4534-EG228026, #1: TRCN0000078808, #2: TRCN0000078809, and nontargeting control: RHS6848) were used according to standard procedures.

Plaque assay

4T1 cells were infected with a low MOI (0.1) of reovirus for 2 hours and were washed to remove nonbound virus, released virus was then collected 24, 48, and 72 hours post infection (h.p.i). Supernatant was collected and titered on L929 cells by standard plaque assay.

Immunofluorescence staining and imaging

Cells were infected with reovirus on coverslips in 12-well dishes. After 24 hours, cells were incubated with 100 nmol/L MitoTracker Deep Red (Thermo Fisher Scientific). Next, cells were washed with PBS and incubated for 20 minutes in 4% paraformaldehyde. Fixed cells were washed with PBS, then permeabilized/blocked in permeabilization buffer (0.1% TritonX-100 and 2% FBS in PBS) for 30 minutes. Afterwards, cells were incubated at room temperature with rat anti-reovirus (generated in-house) for 1 hour, washed with permeabilization buffer, and incubated with FITC anti-rat antibody (Jackson ImmunoResearch Laboratories) for an hour. Coverslips were washed and mounted on glass slides using ProLong Diamond Antifade Mountant (Life Technologies). Imaging was performed at Zeiss Meta510 inverted laser scanning confocal microscope equipped with 488, 543, and 633 nm lasers using 63× Apochromat NA 1.2 objective. Images (1,024 × 1,024 pixels) were captured by Zeiss AxioCam MRc camera. ZEN image acquisition software (Zeiss) was used for image acquisition. Confocal images were acquired as Z-stacks, then compiled into a maximal projection, and analyzed using ImageJ (19).

Statistical analysis

Statistical analysis was done using ANOVA analysis or Kaplan–Meier survival analysis coupled with log-rank test (both with 95% confidence interval). $P < 0.05$ was considered to be statistically significant. Principal component analysis was performed on the normalized proteomics data with R.

Enrichment analysis

All detectable metabolites were organized into specific and general metabolic pathways based on Kyoto Encyclopedia of Genes and Genomes (KEGG) metabolic pathways. To determine pathways that were enriched by reovirus infection or DCA treatment, an overrepresentation analysis was completed. Briefly, metabolites that were increased or decreased by 1.5-fold and t test probability < 0.05 were selected and compared with the original list of metabolites, and then we calculated percent of metabolites changed. We used this percent to calculate the expected number of metabolites that would change if the metabolites were randomly distributed throughout the various metabolic pathways. We then calculated fold enrichment by dividing metabolites changed by 1.5-fold by the number of metabolites expected to have changed if random. Probability was calculated by the hypergeometric test.

Gene ontology term and Interferome analysis

Proteins that were either increased or decreased by 1.5-fold compared with indicated treatment/control were analyzed using the publicly available Panther Classification System using the statistical overrepresentation test. Only pathways that had a FDR < 0.05 were considered. To determine whether targeted proteins were regulated by IFN, the publicly available Interferome database was used.

Results

Virus-induced oxidative stress and central energy metabolism flux correlate with cancer cell sensitivity to oncolysis

Currently, the possible metabolic determinants for OV oncolysis in cancer cells are unknown. To elucidate this, we first performed unbiased metabolomics on reovirus-infected cancer cells, using targeted metabolic profiling with hydrophilic interaction liquid chromatography mass spectrometry (HILIC-MS; ref. 14). For this purpose, we used eight cancer cell lines of varying degrees of susceptibility to reovirus (as determined by oncolysis at 72 h.p.i.; Fig. 1A and B; Supplementary Fig. S1A; Supplementary Tables S1 and S2). It should be noted that a caveat with comparing multiple cell lines is variable infection rates, thus noninfected cells in the population are likely masking metabolic changes (Supplementary Fig. S1B). However, the percent of infected cells at 18 h.p.i. did not correlate with percent oncolysis at 72 h.p.i. (Supplementary Fig. S1C). This is likely because susceptibility of cancer cells to oncolytic reovirus is a multiparameter paradigm (e.g., IFN). At an early timepoint of 24 h.p.i., reovirus infection (MOI 10) induced several cell-dependent changes in intracellular metabolites (Fig. 1A and B). To characterize these changes into pathways, we used overrepresentation analysis on metabolites that were changed by 1.5-fold with a $P < 0.05$ for each KEGG pathway (Supplementary Tables S3 and S4). As shown in Supplementary Fig. S1A, pathways involved in central energy, amino acid, and nucleotide were frequently enhanced. These results captured OV-induced metabolic rewiring within cancers, and pointed toward a possible link between the virus-induced metabolic response and oncolysis.

To identify metabolites associated with the susceptibility of cancer cells to reovirus oncolysis, we correlated the metabolite basal levels with reovirus-mediated oncolysis. Few correlated with reovirus-mediated oncolysis (Supplementary Fig. S1D and S1E; Supplementary Table S5). However, in line with a role for oxidative phosphorylation and glycolysis, we identified basal metabolic characteristics of cancer cells that predict reovirus oncolysis including OCR and ECAR (Fig. 1C and D). Both OCR and ECAR negatively correlate with oncolysis (Fig. 1C and D), suggesting that cancer cells with an inherently higher metabolic activity are more resistant to oncolysis.

To further investigate this link, we correlated reovirus-induced metabolic changes with oncolysis. Indeed, several reovirus-induced metabolite changes correlated with oncolysis (Fig. 1E; Supplementary Table S5). Notably, induction of oxidative stress metabolites, glutathione and glutathione disulfide negatively correlated with oncolysis (Fig. 1F). Also, a negative correlation between an induction of acetyl-CoA, the first metabolite in the TCA cycle or fatty acid synthesis, and oncolysis suggests that the effects of reovirus on central metabolism could determine susceptibility. Furthermore, induction of the TCA cycle intermediate, isocitrate, which is commonly found at high levels in cancer cells with a defective TCA cycle (20), positively correlated with cell death, suggesting the induction of mitochondrial dysfunction during reovirus-mediated oncolysis (Fig. 1E and F). We also, compared the reovirus-induced metabolic changes with percent of infected cells (Supplementary Fig. S1F–S1H). We observed less metabolites that correlated with reovirus infection as compared with oncolysis, however, two that did were glutathione, which positively correlated and the glycolysis intermediate, D-glyceraldehyde 3-phosphate, which negatively correlated with percent infected cells (Supplementary Fig. S1G and S1H). We then examined the effect of reovirus infection on OCR and ECAR, and found that 4T1 and Panc1 had decreased OCR, whereas TRAMPC1 cells had increased OCR after reovirus infection (Fig. 1G and H; Supplementary Fig. S2A). ECAR was increased by reovirus infection in 4T1 and TRAMPC1 cells (Fig. 1I and J; Supplementary Fig. S2B). These reovirus-induced changes on

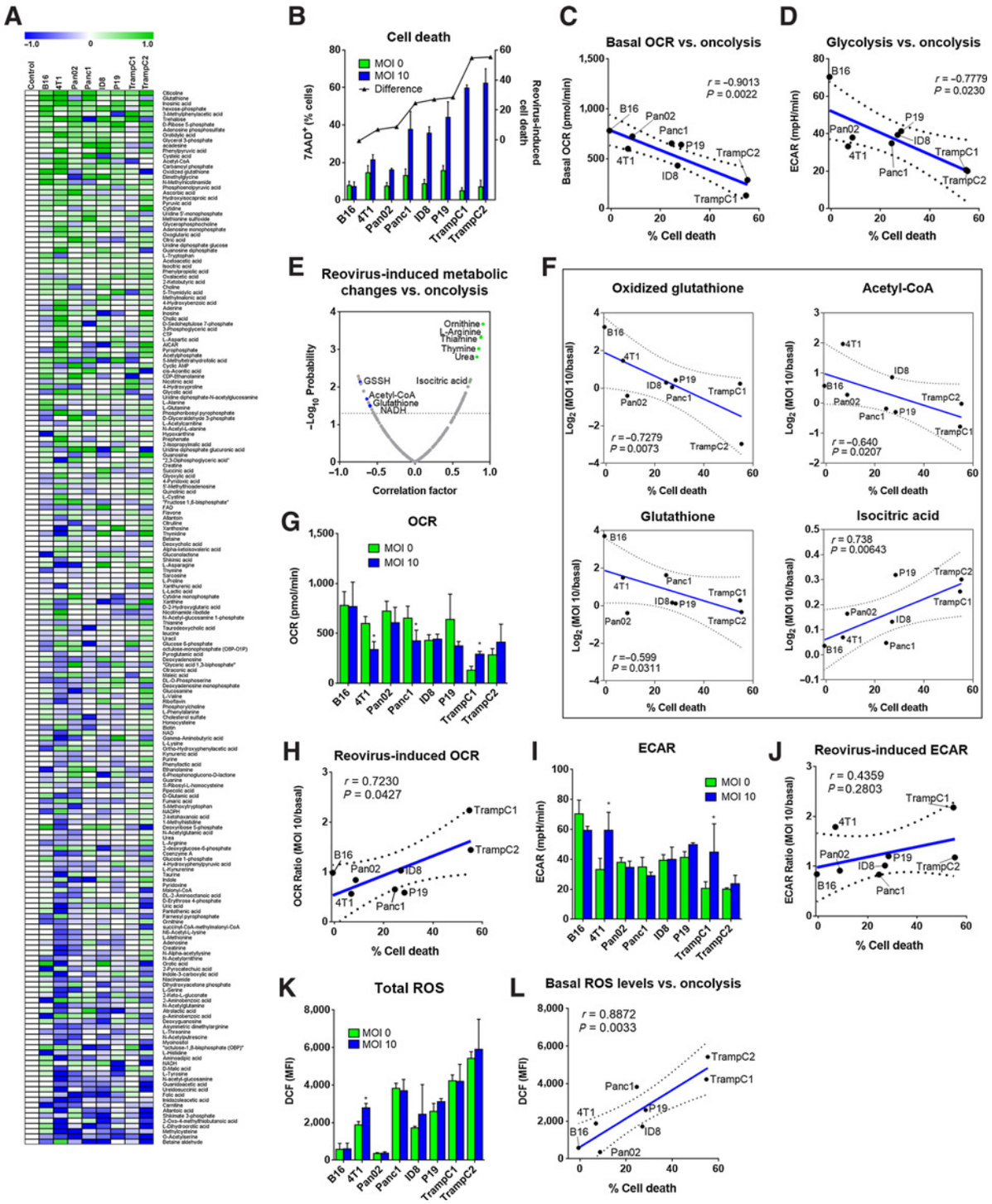

Figure 1.

Oncolytic reovirus alters metabolism in a wide range of cancer cells. HILIC-MS–based metabolomics on cancer cells ± reovirus (MOI 10) 24 h.p.i. **A,** Heatmap representing reovirus-induced metabolite changes. **B,** Percentage of dead cells caused by reovirus (MOI 10), 72 h.p.i. **C,** Correlation between OCR 24 h.p.i and oncolysis (MOI 10) at 72 h.p.i. **D,** Correlation between ECAR 24 h.p.i and oncolysis at 72 h.p.i. **E** and **F,** The correlation value (r) and $-\log_{10}$ probability of reovirus-induced metabolite changes compared with oncolysis (**E**), with examples (**F**). **G,** OCR ± reovirus, 24 h.p.i. **H,** Reovirus-induced OCR at 24 h.p.i. compared with oncolysis at 72 h.p.i. **I.** ECAR ± reovirus, 24 h.p.i. **J,** Reovirus-induced ECAR (24 h.p.i.) compared with oncolysis (72 h.p.i.). **K,** ROS as represented by mean fluorescence intensity (MFI) of DCFH-DA (DCF). **L.** Correlation between basal ROS and oncolysis caused by reovirus (MOI 10) at 72 h.p.i. * $P < 0.05$ as compared with noninfected cells. Values represent mean of at least three independent experiments; error bars, SD.

OCR significantly correlated with reovirus cytotoxicity, whereas reovirus-induced changes on ECAR did not (Fig. 1H–J). To expand the role of oxidative stress in reovirus susceptibility, we measured basal and reovirus-induced ROS (Fig. 1K). Reovirus infection increased ROS only in 4T1 cells, suggesting a unique response by these cells (Fig. 1K). However, basal ROS levels positively correlated with oncolysis (Fig. 1L), suggesting a role for oxidative stress in oncolysis. In summary, unbiased metabolomics and flux analysis identified oxidative stress and central energy metabolism as potential determinants of reovirus oncolysis.

Pharmacologic inhibition of PDKs increases cancer cell susceptibility to reovirus oncolysis

To further elucidate the role of metabolism in oncolysis, we selectively targeted relevant pathways. As illustrated in Supplementary Fig. S2A, we measured the effect of metabolic inhibitors including dichloroacetate (DCA, PDK inhibitor), 2-deoxy-glucose (2DG, hexokinase inhibitor), oligomycin (complex V inhibitor), H_2O_2 (oxidative stress), and etomoxir (carnitine palmitoyltransferase-1 inhibitor) on oncolysis (Fig. 2A and B; Supplementary Fig. S3A and S3B). Indeed, 2DG enhanced oncolysis in Pan02 and TRAMPC2 cells and oligomycin enhanced oncolysis in Pan02 cells as compared with single treatments (Supplementary Fig. S3B). However, DCA produced the largest effect of all the metabolic inhibitors (Fig. 2B). Combination of DCA treatment and reovirus significantly enhanced oncolysis compared with single treatments in B16, 4T1, Panc1, and P19 cells (four of the six cancers that were intrinsically the most resistant toward oncolysis) with the highest extent in 4T1 cells (Fig. 2B; Supplementary Fig. S3B). DCA treatment increased the percentage of reovirus-positive cells in 4T1, TRAMPC1, and TRAMPC2 cells 18 h.p.i. (Supplementary Fig. S3C). Furthermore, direct inhibition of PDH with CPI-613 (Supplementary Fig. S3D and S3E) blocked the synergistic effect by DCA on reovirus cytotoxicity in 4T1 and Panc1 cells (the two cancers that showed the greatest enhancement to oncolysis by DCA; ref. 21; Supplementary Fig. S3F). These findings implicated PDH, the major target for PDK and the regulatory point between glycolysis and TCA cycle, as an important player in reovirus-induced metabolic rewiring and subsequent cytotoxicity.

Furthermore, there was a negative correlation between reovirus-induced inhibitory phosphorylation (at serine 293) of PDH and oncolysis, suggesting that cells able to inhibit PDH upon reovirus infection are best able to resist oncolysis (Fig. 2C–F; refs. 22, 23). In addition, basal PDH/actin levels positively correlated with oncolysis, suggesting cells with higher PDH levels were more susceptible to oncolysis (Fig. 2G). Altogether, these data further support a possible therapeutic utility for targeting PDH activity to enhance the reovirus-induced oncolysis.

Reovirus infection enhances anaerobic glycolysis through an oxidative stress–dependent inhibition of PDH

To specifically understand the mechanism of how PDH activity dictates sensitivity to reovirus-mediated oncolysis we focused on the cancer cell that showed the greatest enhancement to oncolysis by DCA, 4T1. In 4T1 cells, reovirus monotreatment caused oncolysis in less than 5% of cells at 24 h.p.i. (MOI 1, 10, and 100); whereas at 72 h.p.i., reovirus infection (MOI 10) caused 22.1% ± 5.0% cell death (Fig. 3A). To measure early, preoncolysis effects on metabolism by reovirus, we preformed all metabolic experiments at 24 h.p.i. (MOI 1, 10, and 100). In line with Fig. 1, ECAR was increased by reovirus infection at both low and high virus doses (MOI 1 and 10), and extracellular lactate production was increased at MOI 10 (Fig. 3B and C). Similarly, exposure to reovirus enhanced glucose uptake in a concentration-dependent manner (Fig. 3D), further, in these populations, reovirus-infected cells have 3-fold increased glucose uptake compared with noninfected cells (Supplementary Fig. S4A). These changes were accompanied by higher levels of ATP and NADH levels (Fig. 3E). Together showing that reovirus infection caused an early upregulation of glycolytic flux in 4T1 cells. However, reovirus infection decreased basal, maximal, and ATP production–dependent OCR, and spare respiratory capacity and coupling efficiency, suggesting a block at PDH (Fig. 3F; Supplementary Fig. S4B). Consistent with a block at PDH, both pyruvate and lactate levels were increased by reovirus infection (Supplementary Fig. S4C). These results suggested that, following exposure to reovirus, 4T1 cells rewire metabolism through PDH inhibition.

To understand the contribution of cell proteome toward these OV-induced metabolic changes, we performed multi-plex quantitative mass spectrometry–based proteomics on 4T1 cells. As expected, many of the proteomic changes induced by reovirus were IFN-regulated, and involved antiviral processes, protein folding, and response to stress (Supplementary Fig. S4D–S4F; Supplementary Table S6). However, we observed no major changes in protein levels or gene expression of glycolytic or TCA cycle enzymes or no visible mitochondrial structural damage (Supplementary Fig. S4G–S4J; Supplementary Table S6), suggesting that reovirus-induced changes in energy metabolism were most likely regulated through regulatory mechanisms such as phosphorylation. Consistent with findings from Fig. 2C and D, PDH phosphorylation at serine 293 was increased by reovirus infection at MOI 10 (Fig. 3G). Further investigation revealed that out of the four PDKs only *Pdk1* mRNA was upregulated within 24 h.p.i. (Fig. 3H), suggesting a major contribution of PDK1 in reovirus-induced phosphorylation of PDH.

Of note, oxidative stress is one of the major regulators of PDK1 expression (24), suggesting that the reovirus-induced PDK1 expression could occur as a result of oxidative stress. Indeed, reovirus infection increased markers of oxidative stress including levels of superoxide, hydrogen peroxide, glutathione, GSSH, and expression of oxidative stress-sensitive genes (*Nfe2l2* and *SOD2*) (Fig. 3I–L) in 4T1 cells. Next, to confirm our results in an *in vivo* preclinical setting, we performed metabolomics on 4T1 tumors that were treated with a therapeutic regimen of reovirus oncotherapy (Supplementary Fig. S4K; ref. 25). As anticipated, reovirus therapy had marginal effect on the survival of 4T1 tumor–bearing mice (Supplementary Fig. S4L). Indeed, some metabolites, including glutathione, altered by reovirus *in vitro* were similarly altered *in vivo* (Supplementary Fig S4M–S4O; Supplementary Table S7). Thus, further supporting a role for oxidative stress following reovirus infection.

To conclusively show the role of oxidative stress in regulating the inhibitory phosphorylation of PDH, we infected 4T1 cells with reovirus in the presence of the antioxidant, n-acetylcysteine (NAC). As shown in Fig. 3M, NAC impeded the reovirus-induced inhibition of PDH, suggesting that reovirus-induced increase in ROS contributes to the inhibition of PDH in 4T1 cells. Collectively, these data show that reovirus infection caused an oxidative stress–dependent inhibition of PDH, likely mediated

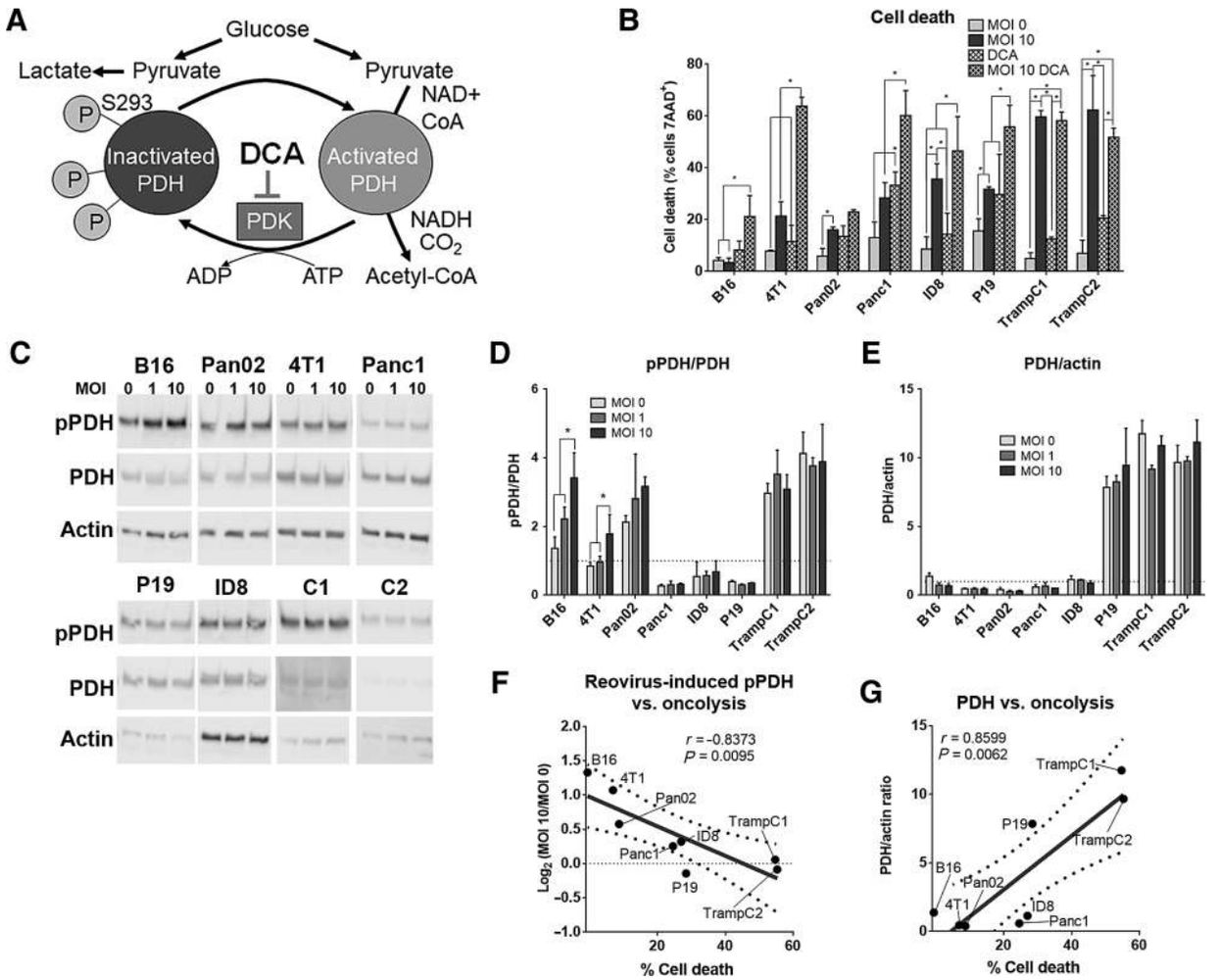

Figure 2.

DCA, a PDK inhibitor, enhances reovirus-induced cytotoxicity in cancer cells. **A,** Schematic representing DCA-mediated inhibition of PDK. **B,** Percentage of dead cells following reovirus infection (MOI 10) ± DCA (20 mmol/L) 72 h.p.i. **C,** Representative immunoblot of pPDH at serine 293, PDH, and actin in cancer cells ± reovirus (MOI 1, 10) 24 h.p.i. **D** and **E,** pPDH/PDH or PDH/actin quantification, with all values normalized to a standard loading control (loading control is represented by a dotted line). Values represent the mean of three independent experiments. **F** and **G,** Reovirus induced changes in pPDH/PDH or PDH/actin at 24 h.p.i. compared with oncolysis at 72 h.p.i. *, $P < 0.05$; error bars, SD.

by PDK1, which contributed to impaired TCA cycle and increased anaerobic glycolysis in 4T1 cells.

DCA augments replication of reovirus and enhances oncolysis through oxidative stress in 4T1 cells

Because 4T1 cells are relatively resistant to reovirus-oncolysis, we hypothesized that the oxidative stress–induced inhibition of PDH (as described in Fig. 3) aids the establishment of cancer cell fitness against infection and oncolysis. Indeed, as shown in Fig. 2, while DCA or reovirus monotreatments cause minimal effect on cell survival, the combination of DCA and reovirus makes 4T1 cells extensively susceptible to cell death. To examine the mechanism of this synergistic between DCA/reovirus combination we first analyzed the activity of PDKs, by assessing the phosphorylation of PDH. As expected, DCA treatment (5 and 20 mmol/L for 24 hours) not only decreased PDH phosphorylation on its own, but also blocked reovirus-induced increase pPDH (Fig. 4A, first subpanel). It should be noted that changes in pPDH occur independent of the changes in protein expression (Fig. 4A, second subpanel). Furthermore, confirming our earlier findings, oncolysis was enhanced by the combination of DCA and active reovirus (but not UV-inactivated virus or IFNα), compared with reovirus or DCA alone, at 48 and 72 h.p.i. (Fig. 4B; Supplementary Fig. S5A).

To determine whether the effects of DCA were specific to PDK, we specifically depleted PDK1, using shRNA (Supplementary Fig. S5B). In keeping with the effect of DCA on PDK1, oncolysis was enhanced by PDK1 knockdown (KD) in both shRNAs examined compared with control (Supplementary Fig. S5C). Interestingly, DCA only caused a small, nonsignificant enhancement of reovirus-mediated cytotoxicity in PDK1 KD cells, suggesting that the effects of DCA are primarily mediated through PDK1 and that the other PDK isoforms or other putative non-PDK targets of DCA have minimal role in our

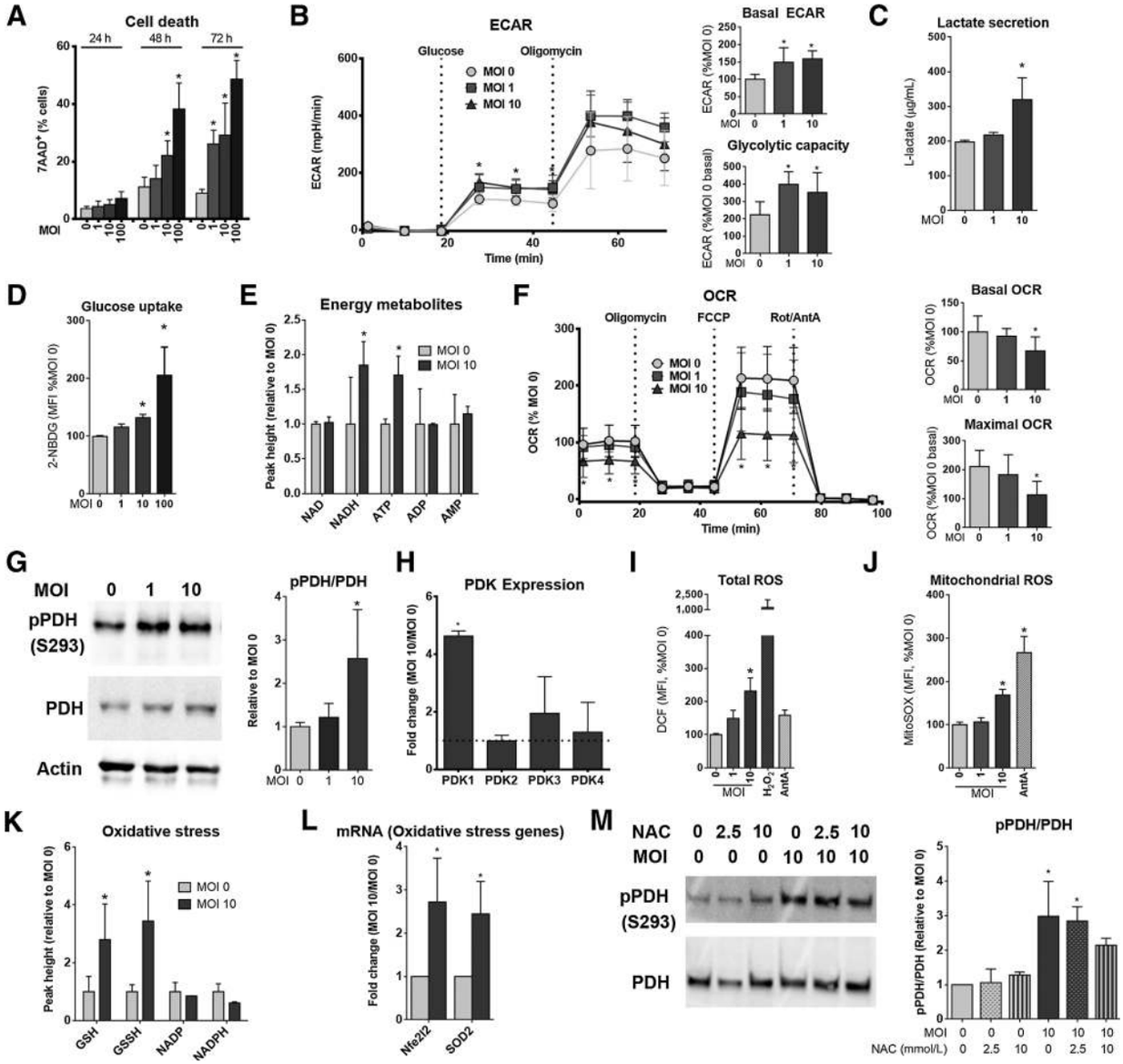

Figure 3.

Reovirus infection causes an oxidative stress–dependent inhibition of PDH in 4T1 cells. **A,** Percentage of dead cells following reovirus infection (MOI 1, 10, or 100) compared with control (MOI 0), 24, 48, or 72 h.p.i. **B,** ECAR of 4T1 cells infected ± reovirus (MOI 0, 1, or 10) 24 h.p.i. after subsequent injections of glucose and oligomycin. **C,** Extracellular lactate production by 4T1 cells, cultured ± reovirus (MOI 1 or 10) 24 h.p.i. **D,** MFI of 2-NBDG uptake in 30 minutes by 4T1 cells ± reovirus (MOI 1, 10, or 100) 24 h.p.i. **E,** Relative metabolite levels normalized against noninfected 4T1 cells (MOI 0). **F,** OCR of 4T1 cells infected ± reovirus (MOI 1 or 10) 24 h.p.i. after subsequent injections of oligomycin, FCCP, and a combination of rotenone and antimycin A. **G,** Representative immunoblot of pPDH, PDH, and actin in 4T1 cells treated ± reovirus (MOI 1 or 10). pPDH/PDH quantification. **H,** mRNA levels of *Pdk1-4* after reovirus infection compared with noninfected cells (dotted line) normalized per GAPDH mRNA levels. Total (**I**) and mitochondrial (**J**) ROS. Treatment (30 minutes) of 4T1 cells with hydrogen peroxide (1 mmol/L) and antimycin A (5 μmol/L, AntA) as positive controls. **K,** Relative metabolite levels normalized against noninfected 4T1 cells. **L,** mRNA levels normalized per GAPDH mRNA levels. **M,** Representative immunoblot of pPDH, total PDH, and actin in 4T1 cells treated with or without reovirus (MOI 10) ± NAC (2.5 or 10 mmol/L). Bar graph quantifying pPDH/PDH. *, $P < 0.05$ as compared with noninfected cells. Bar graphs, the means of a minimum of three independent experiments; error bar, SD.

system (Supplementary Fig. S5C). Supporting this hypothesis, treatment of 4T1 cells with a PDK1/2-specific inhibitor, AZD7545, prevented pPDH and synergistically increased oncolysis (refs. 26, 27; Supplementary Fig. S5D and S5E). Together, these experiments strongly suggested the enhanced cytotoxicity of DCA/reovirus combination treatment is mediated through DCA's inhibitory effect on PDK1.

To address whether enhanced susceptibility of cancer cells to DCA/reovirus was supported through increased OV infection or replication, we measured the percentage of cells infected by

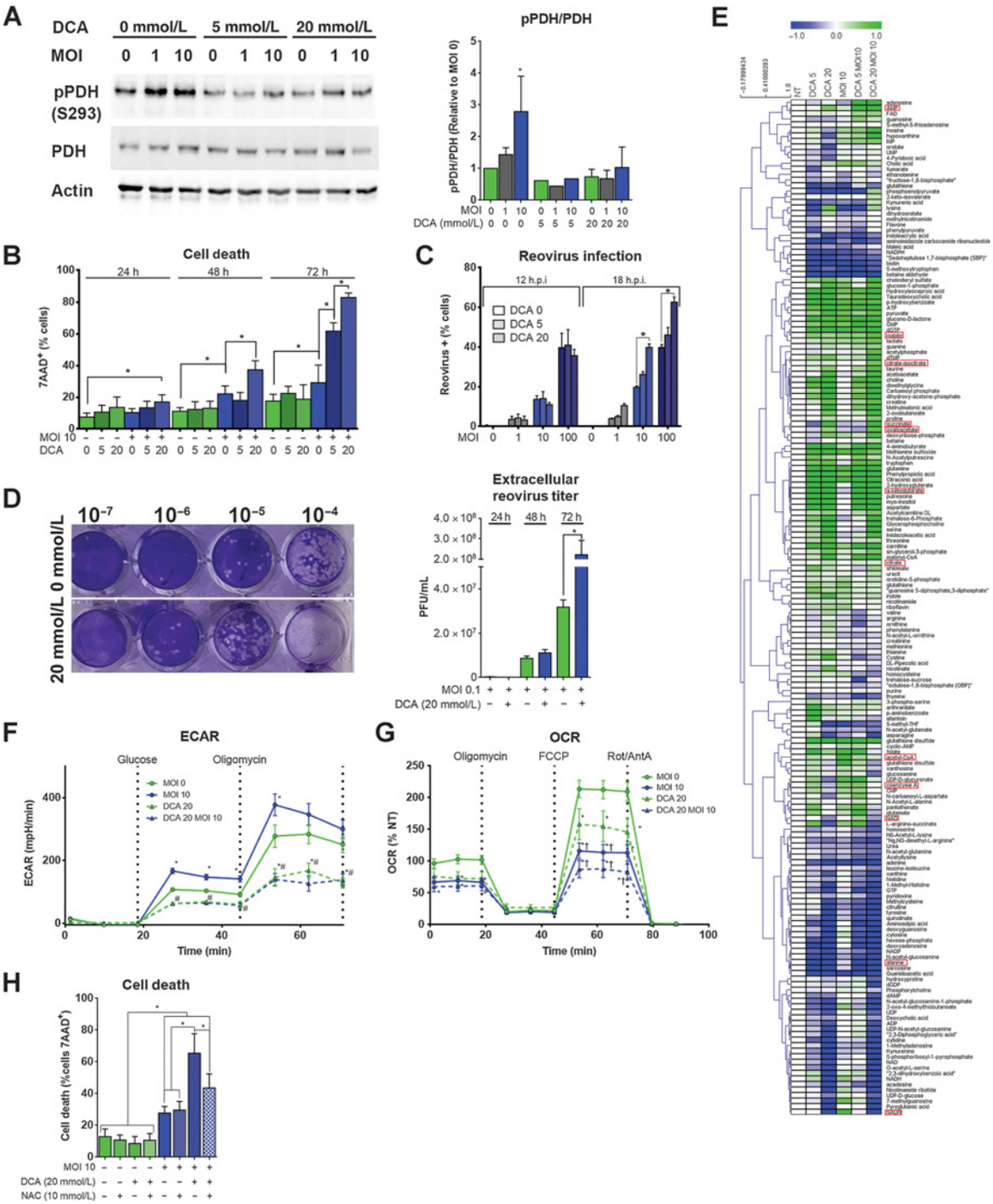

Figure 4.

Dichloroacetate prevented reovirus-induced increase in glycolysis and enhanced the efficacy of oncolysis in an oxidative stress–dependent mechanism. **A,** Representative immunoblot detecting levels of pPDH, total PDH, and actin in 4T1 cells treated ± reovirus (MOI 1 10) in combination ± DCA (5 or 20 mmol/L) for 24 hours. pPDH/PDH levels quantitated and normalized to nontreated cells. **B,** Cell death analysis of 4T1 cells treated ± reovirus (MOI 10) in combination ± DCA (5 or 20 mmol/L) for 24, 48, or 72 hours. **C,** Percent of 4T1 cells that were infected with reovirus 12 and 18 h.p.i. **D,** Extracellular reovirus titer of conditioned media from 4T1 cells, ± reovirus (MOI 0.1) for 24, 48, or 72 hours. A representative image of crystal violet–stained L cells from 72 h.p.i. The dilution range of 10^{-7}–10^{-4} is shown. **E,** Metabolite levels of 4T1 cells treated with DCA (5 or 20 mmol/L) and infected with reovirus (MOI 10), 24 h.p.i., are represented by a heatmap. Metabolites highlighted by a red rectangle are discussed in the text. **F,** ECAR of 4T1 cells infected ± reovirus (MOI 10) in combination ± DCA (20 mmol/L) for 24 hours after subsequent injections of glucose and oligomycin. **G,** OCR of 4T1 cells ± reovirus (MOI 10) ± DCA (20 mmol/L) for 24 hours after subsequent injections of oligomycin, FCCP, and a combination of rotenone and antimycin A. **H,** Cell death of 4T1 cells infected ± reovirus (MOI 10) and ± DCA (20 mmol/L) ± NAC (10 mmol/L). *, $P < 0.05$. Bar graphs, the means of a minimum of three independent experiments; error bars SD.

reovirus at 12 and 18 h.p.i. At the prereplication timepoint of 12 h.p.i., we observed no difference in the percentage of infected cells between cells treated ± DCA (Fig. 4C; ref. 6). However, at 18 h.p.i., which represents one round of replication, reovirus-infected cells were higher in the presence of DCA as compared with control, over a range of MOIs, indicating that DCA enhances the replication of reovirus in 4T1 cells (Fig. 4C). Similarly, PDK1 KD increased the percentage of reovirus-infected cells at 18 h.p.i. (Supplementary Fig. S5F). Next, we asked whether DCA influenced extracellular reoviral titer in 4T1 72 h.p.i. When analyzed in plaque forming assay, DCA-treated 4T1s produced higher titers of reovirus, compared with controls (Fig. 4D). Such increased release of infectious particles is in concordance with increased oncolysis observed through the combination of DCA and reovirus.

To understand the mechanism behind DCA-promoted OV replication, we evaluated the effect of DCA on whole proteome of reovirus-infected 4T1 cells. DCA treatment alone had minimal effect on the proteome but in combination with reovirus, DCA caused several changes compared with either single treatment (Supplementary Fig. S5G–S5N; Supplementary Table S6). In addition, AZD7545 in combination with reovirus had a similar effect on 4T1 proteome as DCA combined with reovirus, further confirming that DCA's effects were caused by PDK inhibition and not by off target effects (Supplementary Fig. S4O). Consistent with increased viral replication, all reovirus proteins detected by proteomics were increased by DCA or AZD7545 (Supplementary Fig. S5P and S5Q). Compared with reovirus treatment, combination with DCA enhanced the levels of 67 proteins (by at least 1.5-fold) involved in viral processing, response to IFNγ, carbohydrate metabolic processes, and response to stress (Supplementary Fig. S5G and S5R). In addition, DCA had no obvious negative effect on the reovirus-induced upregulation of *Ifna1* or IFN-regulated genes (*Isg56*, *Ddx58*/*Rig-I*, and *IL6*) expression (Supplementary Fig. S5S–S5V). Together these data show that, during DCA/reovirus combination treatment, antiviral defense remained functional and thus did not contribute to increased viral replication.

To determine whether the cell death mechanism by combination treatment was at the enzymatic activity level, we performed metabolomics on 4T1 cells treated ± reovirus and ± DCA (Fig. 4E; Supplementary Table S8). In agreement with decreased glycolysis and increased TCA cycle flux, DCA alone caused many metabolic changes including increased alpha-ketoglutarate, and decreased NAD^+, NADH, and alanine (Fig. 4E; Supplementary Table S8). DCA also prevented the reovirus-induced increases in the PDH metabolites acetyl-CoA and coenzyme A, and prevented the decrease in TCA cycle intermediates succinate, oxaloacetate, malate, and citrate (Fig. 4E). These changes support our model where reovirus infection inhibits PDH in 4T1 cells, and DCA overrides this inactivation. Also, and in line with literature (28), DCA treatment alone decreased glucose uptake, ECAR, and maximal ECAR levels and was sufficient to prevent reovirus-induced increased glucose uptake and ECAR (Fig. 4F; Supplementary S6A–S6C). DCA treatment alone had minimal effects on OCR and did not prevent reovirus-induced inhibition of OCR (Fig. 4G; Supplementary Fig. S6D and S6E). Interestingly, maximal OCR was decreased by reovirus alone and not rescued by combination of DCA and reovirus, suggesting that reovirus infection caused other unknown mitochondrial dysfunction in addition to blocking PDH activity (Supplementary Fig. S6E). A phenogram summarizing ECAR and OCR shows that reovirus infection alone caused 4T1 cells to become glycolytic, whereas combination of DCA and reovirus caused cells to become metabolically quiescent (Supplementary Fig. S6F). Altogether our findings suggest that the cause of enhanced oncolysis with DCA/reovirus combination stems from metabolic perturbations. Specifically, reovirus initially damaged the mitochondria causing ROS, to which 4T1 cells respond by blocking PDH. Subsequent addition of DCA to reactivate PDH bypasses the cells' metabolic fitness mechanism and leads to cell death.

To test this hypothesis, we investigated the effect of blocking oxidative stress during the DCA/reovirus combination treatment. Indeed, treatment with NAC in combination with reovirus and DCA, reduced the effects of DCA/reovirus on 4T1 cell death without affecting intracellular reovirus levels (Fig. 4H; Supplementary Fig. S6G). This shows that oxidative stress contributed to oncolysis during combinational treatment by either direct killing or by priming 4T1 cells (e.g., pPDH) to become sensitive to DCA-mediated metabolic changes, during reovirus oncotherapy.

In vivo, DCA enhances the antitumor efficacy of reovirus-based cancer therapy

To determine the clinical applicability of our findings, we tested whether the *in vitro* synergistic effect of reovirus and DCA on cancer cell death was translatable *in vivo*. For this purpose, 4T1-xenografted tumor-bearing immunocompromised mice were injected intratumorally three times with PBS, DCA, and/or reovirus, and supplied with DCA or water control in drinking water (Fig. 5A). All the animals were then monitored for tumor growth and survival. In line with our *in vitro* results, reovirus alone significantly enhanced survival but mice treated with a combination of DCA/reovirus showed significantly better survival, as compared with mice treated with the monotherapies of DCA and reovirus, or PBS alone (Fig. 5B). Also, tumor volume was significantly smaller in 4T1 tumor–bearing mice injected with the combination therapy as compared with mice injected with PBS, DCA, or reovirus alone (Supplementary Fig. S6H). These results demonstrated that DCA enhances the antitumor efficacy of oncolytic reovirus–based cancer therapy in preclinical settings.

Finally, because immune system plays an important role in cancer therapies, particularly with oncolytic viruses, we expanded our findings into a syngeneic immunocompetent mouse model (Fig. 5A; ref. 25). Similar to the data obtained from xenografted immunodeficient mice above, the combination of DCA and reovirus treatment significantly improved the life span of 4T1-bearing Balb/c mice compared with the DCA/reovirus monotherapies, or PBS (Fig. 5C). Despite the modest increase in survival, tumor volume did not differ between reovirus and combination injected mice, suggesting that the combinational treatment effects were not as pronounced in an immunocompetent model as compared with an immunocompromised model (Supplementary Fig. S6I). To confirm this finding, we repeated the tumor experiment using 15 mice per treatment (Supplementary Fig. S6J and S6K). Nevertheless, these findings still showed that DCA effective at promoting better efficacy for reovirus-based cancer therapy in immunocompetent mice. Collectively, these results from preclinical testing conclusively showed the translational promise for combining PDK inhibition with oncolytic reovirus to promote better outcomes from cancers in clinics.

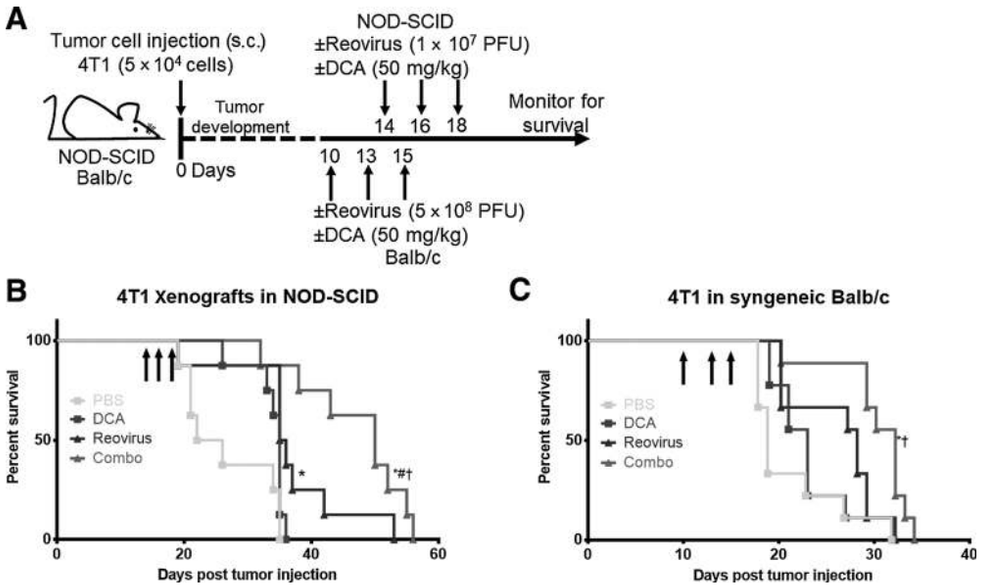

Figure 5.

DCA enhanced the antitumor efficacy of reovirus-based cancer therapy *in vivo*. **A,** Schematic representing the time-line and experimental procedures used during animal experiments. **B,** Survival analysis of 4T1 tumor–bearing NOD-SCID mice after the injection of reovirus and/or DCA, alone or in combination with each other (arrows). **C,** Survival analysis of 4T1 tumor–bearing Balb/c mice after the injection of reovirus and/or DCA, alone or in combination with each other (arrows). A minimum of 8 mice in each treatment group were used. *, $P < 0.05$ compared with PBS treated; #, $P < 0.05$ compared with reovirus-only treated; †, $P < 0.05$ compared with DCA-only treated.

Discussion

Here, we demonstrate that therapy-induced metabolic perturbations within cancer cells can be selectively reprogrammed to enhance the antitumor effects of oncolytic reovirus-based cancer therapy. To test this paradigm, we aimed to (i) determine the effect of oncolytic reovirus infection on cancer metabolism, and to (ii) explore whether we could exploit these metabolic perturbations to enhance reovirus-induced oncolysis. Using metabolomics and biochemical assays (Fig. 1) on a panel of cancer cell lines, we measured the effect of reovirus infection on metabolism. Several basal- and reovirus-induced metabolic changes, most notably in central energy metabolism and oxidative stress, correlated with sensitivity to reovirus cytotoxicity (Figs. 1C–F, H, L, and M, 2F and G), suggesting these metabolic pathways can be fine-tuned for achieving enhanced oncolysis in cancer cells (Figs. 2B and 4B).

Our data strongly suggest that mitochondrial function plays a role in sensitivity to reovirus oncolysis. A role for mitochondrial function is already known in other viral infections including KSHV, which decreased oxidative phosphorylation upon infection, and HCMV and Sindbis virus, both of which increased oxidative phosphorylation (29–31). In line with our 4T1 data, other viruses including vaccinia virus, hepatitis C virus, and influenza A (H1N1) inhibit PDH activity through increased expression of PDK1 in HEK293T cells, PDK1 and 3 in hepatocytes, and PDK4 in mice, respectively (32–34).

To determine whether reovirus-induced inhibition of PDH was a possible protective antideath mechanism employed by the host cancer cells, we reactivated PDH with pharmacologic inhibition of PDKs using DCA-, AZD7545-, or shRNA-mediated depletion of PDK1. These conditions reduced reovirus-induced PDH phosphorylation, resulting in the flux of pyruvate toward the TCA cycle and away from lactate production (Fig. 4A, E–G; Supplementary Fig. S6B and S6D; ref. 28). Such PDK1 inhibition–induced perturbations possibly established metabolic fitness of cancer cells during reovirus infection, causing enhanced oncolysis in combination with reovirus (Fig. 4B, F, and G; Supplementary Figs. S5C and S5E, and S6F). Our findings are similar to previous studies showing beneficial effects of DCA when combined with genetically modified adenovirus and measles (35, 36). On the other hand, our findings contrast with studies showing detrimental effects of PDK4 inhibition in influenza infection, and of DCA treatment on hepatitis C viral replication, indicating that PDH plays different roles depending on the virus and cell type (32, 33). It is noteworthy that, despite the known antitumor effects of DCA in a wide range of cancer cells *in vitro* and *in vivo*, 4T1 cells are resistant to DCA or AZD7545 treatment or PDK1 depletion (Fig. 4B; refs. 28, 37, 38; Supplementary Fig. S5C and S5E). Interestingly, it has been reported that DCA selectively targets cells with defects in the mitochondrial electron transport chain (39). Along these lines, we found that DCA killed 4T1 cells only when combined with reovirus, which caused decreased mitochondrial function (that was not rescued by DCA treatment; Figs. 3I–L and 4G), suggesting that reovirus-induced mitochondrial dysfunction was required for DCA-dependent cell death in 4T1 cells. However, we could not detect any defects in mitochondrial structure or mitochondrial protein levels, other than increased phosphorylation of PDH (Fig. 3G; Supplementary Fig. S4I and S4J), suggesting that inhibition of PDH, which is known to induce ROS production (40), is an early event in establishing reovirus resistance in 4T1 cells. These, along with our data that NAC partially blocks PDH phosphorylation, suggests a model that reovirus targets PDH in an unknown

mechanism, inducing ROS production, which further contributes to PDH inhibition.

In conclusion, our data shows that pharmacologic and genetic inhibition of PDK enhanced the efficacy of reovirus cancer therapy through compromising metabolic fitness and oxidative stress in cancer cells. Our comprehensive metabolome/proteome analysis captures novel implications for PDH in oncolytic reovirus–mediated oncolysis of cancer cells, and advocates for combining OV therapies with targeted metabolic reprogramming of cancer cells through pharmacologic interventions. This study shows that a better understanding of OV-induced metabolic changes holds the key to enhancing the therapeutic efficacy of OV-based cancer therapies in clinics.

Disclosure of Potential Conflicts of Interest

N. Holay has ownership interest (including stock, patents, etc.) in Oncolytics Biotech. No potential conflicts of interest were disclosed by the other authors.

Authors' Contributions

Conception and design: B.E. Kennedy, S. Gujar
Development of methodology: B.E. Kennedy, J.P. Murphy, D.R. Clements, G.P. Pathak, S. Gujar
Acquisition of data (provided animals, acquired and managed patients, provided facilities, etc.): B.E. Kennedy, J.P. Murphy, D.R. Clements, N. Holay, G.P. Pathak, Y.E. Hiani, S. Gujar
Analysis and interpretation of data (e.g., statistical analysis, biostatistics, computational analysis): B.E. Kennedy, J.P. Murphy, P. Konda, N. Holay, M.A. Giacomantonio, S. Gujar
Writing, review, and/or revision of the manuscript: B.E. Kennedy, Y. Kim, G.P. Pathak, M.A. Giacomantonio, S. Gujar
Administrative, technical, or material support (i.e., reporting or organizing data, constructing databases): B.E. Kennedy, J.P. Murphy, G.P. Pathak, S. Gujar
Study supervision: S. Gujar
Other (funding): S. Gujar

Acknowledgments

We thank Alejandro Cohen for mass spectrometry help and Nadia Farbstein for animal work. This work was supported by Canadian Institutes of Health Research (CIHR), Canadian Cancer Society Research Institute, and Terry Fox Research Institute (TFRI). B.E. Kennedy and J.P. Murphy are funded by Beatrice Hunter Cancer Research Institute's (BHCRI) Cancer Research Training Program (CRTP), with B.E. Kennedy's support coming from TFRI and Dalhousie Medical Research Foundation (DMRF). M.A. Giacomantonio is funded by BHCRI CRTP program with funds provided by QEII Health Sciences Centre Foundation and GIVETOLIVE Becky Beaton Award. D.R. Clements and Y. Kim are funded by CIHR, P. Konda and N. Holay are funded by Nova Scotia Graduate Scholarship, and S. Gujar is supported by DMRF.

The costs of publication of this article were defrayed in part by the payment of page charges. This article must therefore be hereby marked *advertisement* in accordance with 18 U.S.C. Section 1734 solely to indicate this fact.

Received August 7, 2018; revised February 27, 2019; accepted May 10, 2019; published first May 14, 2019.

References

1. Pol J, Kroemer G, Galluzzi L. First oncolytic virus approved for melanoma immunotherapy. Oncoimmunology 2016;5:e1115641.
2. Coffey MC, Strong JE, Forsyth PA, Lee PW. Reovirus therapy of tumors with activated Ras pathway. Science 1998;282:1332–4.
3. Hingorani P, Zhang W, Lin J, Liu L, Guha C, Kolb EA. Systemic administration of reovirus (Reolysin) inhibits growth of human sarcoma xenografts. Cancer 2011;117:1764–74.
4. Shmulevitz M, Pan LZ, Garant K, Pan D, Lee PW. Oncogenic Ras promotes reovirus spread by suppressing IFN-beta production through negative regulation of RIG-I signaling. Cancer Res 2010;70:4912–21.
5. Ikeda Y, Nishimura G, Yanoma S, Kubota A, Furukawa M, Tsukuda M. Reovirus oncolysis in human head and neck squamous carcinoma cells. Auris Nasus Larynx 2004;31:407–12.
6. Marcato P, Shmulevitz M, Pan D, Stoltz D, Lee PW. Ras transformation mediates reovirus oncolysis by enhancing virus uncoating, particle infectivity, and apoptosis-dependent release. Mol Ther 2007;15:1522–30.
7. Ackermann WW, Klernschmidt E. Concerning the relation of the Krebs cycle to virus propagation. J Biol Chem 1951;189:421–8.
8. Burke JD, Platanias LC, Fish EN. Beta interferon regulation of glucose metabolism is PI3K/Akt dependent and important for antiviral activity against coxsackievirus B3. J Virol 2014;88:3485–95.
9. Jiang H, Shi H, Sun M, Wang Y, Meng Q, Guo P, et al. PFKFB3-driven macrophage glycolytic metabolism is a crucial component of innate antiviral defense. J Immunol 2016;197:2880–90.
10. Bachmanov AA, Reed DR, Beauchamp GK, Tordoff MG. Food intake, water intake, and drinking spout side preference of 28 mouse strains. Behav Genet 2002;32:435–43.
11. Yaromina A, Meyer S, Fabian C, Zaleska K, Sattler UG, Kunz-Schughart LA, et al. Effects of three modifiers of glycolysis on ATP, lactate, hypoxia, and growth in human tumor cell lines *in vivo*. Strahlenther Onkol 2012;188:431–7.
12. Smith RE, Zweerink HJ, Joklik WK. Polypeptide components of virions, top component and cores of reovirus type 3. Virology 1969;39:791–810.
13. Roby KF, Taylor CC, Sweetwood JP, Cheng Y, Pace JL, Tawfik O, et al. Development of a syngeneic mouse model for events related to ovarian cancer. Carcinogenesis 2000;21:585–91.
14. Yuan M, Breitkopf SB, Yang X, Asara JM. A positive/negative ion-switching, targeted mass spectrometry-based metabolomics platform for bodily fluids, cells, and fresh and fixed tissue. Nat Protoc 2012;7:872–81.
15. Murphy JP, Stepanova E, Everley RA, Paulo JA, Gygi SP. Comprehensive temporal protein dynamics during the diauxic shift in *Saccharomyces cerevisiae*. Mol Cell Proteomics 2015;14:2454–65.
16. Rappsilber J, Ishihama Y, Mann M. Stop and go extraction tips for matrix-assisted laser desorption/ionization, nanoelectrospray, and LC/MS sample pretreatment in proteomics. Anal Chem 2003;75:663–70.
17. Ting L, Rad R, Gygi SP, Haas W. MS3 eliminates ratio distortion in isobaric multiplexed quantitative proteomics. Nat Methods 2011;8:937–40.
18. Livak KJ, Schmittgen TD. Analysis of relative gene expression data using real-time quantitative PCR and the 2(-Delta Delta C(T)) method. Methods 2001;25:402–8.
19. Schneider CA, Rasband WS, Eliceiri KW. NIH image to ImageJ: 25 years of image analysis. Nat Methods 2012;9:671–5.
20. Reitman ZJ, Yan H. Isocitrate dehydrogenase 1 and 2 mutations in cancer: alterations at a crossroads of cellular metabolism. J Natl Cancer Inst 2010;102:932–41.
21. Zachar Z, Marecek J, Maturo C, Gupta S, Stuart SD, Howell K, et al. Non-redox-active lipoate derivates disrupt cancer cell mitochondrial metabolism and are potent anticancer agents *in vivo*. J Mol Med 2011;89:1137–48.
22. Korotchkina LG, Patel MS. Site specificity of four pyruvate dehydrogenase kinase isoenzymes toward the three phosphorylation sites of human pyruvate dehydrogenase. J Biol Chem 2001;276:37223–9.
23. Kolobova E, Tuganova A, Boulatnikov I, Popov KM. Regulation of pyruvate dehydrogenase activity through phosphorylation at multiple sites. Biochem J 2001;358:69–77.
24. Chang CW, Chen YS, Tsay YG, Han CL, Chen YJ, Yang CC, et al. ROS-independent ER stress-mediated NRF2 activation promotes Warburg effect to maintain stemness-associated properties of cancer-initiating cells. Cell Death Dis 2018;9:194.
25. Gujar SA, Marcato P, Pan D, Lee PW. Reovirus virotherapy overrides tumor antigen presentation evasion and promotes protective antitumor immunity. Mol Cancer Ther 2010;9:2924–33.

26. Kato M, Li J, Chuang JL, Chuang DT. Distinct structural mechanisms for inhibition of pyruvate dehydrogenase kinase isoforms by AZD7545, dichloroacetate, and radicicol. Structure 2007;15:992–1004.
27. Morrell JA, Orme J, Butlin RJ, Roche TE, Mayers RM, Kilgour E. AZD7545 is a selective inhibitor of pyruvate dehydrogenase kinase 2. Biochem Soc Trans 2003;31:1168–70.
28. Bonnet S, Archer SL, Allalunis-Turner J, Haromy A, Beaulieu C, Thompson R, et al. A mitochondria-K+ channel axis is suppressed in cancer and its normalization promotes apoptosis and inhibits cancer growth. Cancer Cell 2007;11:37–51.
29. Delgado T, Carroll PA, Punjabi AS, Margineantu D, Hockenbery DM, Lagunoff M. Induction of the Warburg effect by Kaposi's sarcoma herpesvirus is required for the maintenance of latently infected endothelial cells. Proc Natl Acad Sci U S A 2010;107: 10696–701.
30. Kaarbo M, Ager-Wick E, Osenbroch PO, Kilander A, Skinnes R, Muller F, et al. Human cytomegalovirus infection increases mitochondrial biogenesis. Mitochondrion 2011;11:935–45.
31. Silva da Costa L, Pereira da Silva AP, Da Poian AT, El-Bacha T. Mitochondrial bioenergetic alterations in mouse neuroblastoma cells infected with Sindbis virus: implications to viral replication and neuronal death. PLoS One 2012;7:e33871.
32. Yamane K, Indalao IL, Chida J, Yamamoto Y, Hanawa M, Kido H. Diisopropylamine dichloroacetate, a novel pyruvate dehydrogenase kinase 4 inhibitor, as a potential therapeutic agent for metabolic disorders and multiorgan failure in severe influenza. PLoS One 2014; 9:e98032.
33. Jung GS, Jeon JH, Choi YK, Jang SY, Park SY, Kim SW, et al. Pyruvate dehydrogenase kinase regulates hepatitis C virus replication. Sci Rep 2016; 6:30846.
34. Mazzon M, Peters NE, Loenarz C, Krysztofinska EM, Ember SW, Ferguson BJ, et al. A mechanism for induction of a hypoxic response by vaccinia virus. Proc Natl Acad Sci U S A 2013;110:12444–9.
35. Xiao L, Li X, Niu N, Qian J, Xie G, Wang Y. Dichloroacetate (DCA) enhances tumor cell death in combination with oncolytic adenovirus armed with MDA-7/IL-24. Mol Cell Biochem 2010;340:31–40.
36. Li C, Meng G, Su L, Chen A, Xia M, Xu C, et al. Dichloroacetate blocks aerobic glycolytic adaptation to attenuated measles virus and promotes viral replication leading to enhanced oncolysis in glioblastoma. Oncotarget 2015;6:1544–55.
37. Sun RC, Fadia M, Dahlstrom JE, Parish CR, Board PG, Blackburn AC. Reversal of the glycolytic phenotype by dichloroacetate inhibits metastatic breast cancer cell growth in vitro and in vivo. Breast Cancer Res Treat 2010; 120:253–60.
38. Dupuy F, Tabaries S, Andrzejewski S, Dong Z, Blagih J, Annis MG, et al. PDK1-dependent metabolic reprogramming dictates metastatic potential in breast cancer. Cell Metab 2015;22:577–89.
39. Stockwin LH, Yu SX, Borgel S, Hancock C, Wolfe TL, Phillips LR, et al. Sodium dichloroacetate selectively targets cells with defects in the mitochondrial ETC. Int J Cancer 2010;127:2510–9.
40. Stuart SD, Schauble A, Gupta S, Kennedy AD, Keppler BR, Bingham PM, et al. A strategically designed small molecule attacks alpha-ketoglutarate dehydrogenase in tumor cells through a redox process. Cancer Metab 2014; 2:4.